ORIGINAL ARTICLE

Skin inflammation and impaired adipogenesis in a mouse model of acid ceramidase deficiency

Jitka Rybova[1] | Ladislav Kuchar[2] | Jakub Sikora[2,3] |
William M. McKillop[1] | Jeffrey A. Medin[1,4]

[1]Departments of Pediatrics and Biochemistry, Medical College of Wisconsin, Milwaukee, Wisconsin, USA

[2]Rare Diseases Research Unit, Department of Pediatrics and Inherited Metabolic Disorders, Charles University, 1st Faculty of Medicine and General University Hospital, Prague, Czech Republic

[3]Institute of Pathology, Charles University, 1st Faculty of Medicine and General University Hospital, Prague, Czech Republic

[4]Department of Biochemistry, Medical College of Wisconsin, Milwaukee, Wisconsin, USA

Correspondence
Jeffrey A. Medin, Departments of Pediatrics and Biochemistry, Medical College of Wisconsin, Milwaukee, WI, USA.
Email: jmedin@mcw.edu

Abstract

Acid ceramidase catalyzes the degradation of ceramide into sphingosine and a free fatty acid. Acid ceramidase deficiency results in lipid accumulation in many tissues and leads to the development of Farber disease (FD). Typical manifestations of classical FD include formation of subcutaneous nodules and joint contractures as well as the development of a hoarse voice. Healthy skin depends on a unique lipid profile to form a barrier that confers protection from pathogens, prevents excessive water loss, and mediates cell–cell communication. Ceramides comprise ~50% of total epidermis lipids and regulate cutaneous homeostasis and inflammation. Abnormal skin development including visual skin lesions has been reported in FD patients, but a detailed study of FD skin has not been performed. We conducted a pathophysiological study of the skin in our mouse model of FD. We observed altered lipid composition in FD skin dominated by accumulation of all studied ceramide species and buildup of abnormal storage structures affecting mainly the dermis. A deficiency of acid ceramidase activity also led to the activation of inflammatory IL-6/JAK/signal transducer and activator of transcription 3 and noncanonical NF-κB signaling pathways. Last, we report reduced proliferation of FD mouse fibroblasts and adipose-derived stem/stromal cells (ASC) along with impaired differentiation of ASCs into mature adipocytes.

KEYWORDS
acid ceramidase, adipogenesis, ceramides, Farber disease, macrophages, skin

1 | INTRODUCTION

Farber disease (FD) is an ultrarare inherited lysosomal storage disorder caused by mutations in the *ASAH1* gene that encodes the lysosomal hydrolase acid ceramidase (*N*-acylsphingosine amidohydrolase 1, ACDase). ACDase normally catalyzes the degradation of bioactive ceramides (Cer) into sphingosine (SPH) and free fatty acids. FD is often lethal in childhood, and presents as a multisystem disorder with a variable clinical phenotype.[1] Typical formation of subcutaneous nodules, granulomatous collections of storage laden cells and fibrous adipose tissue (AT) are often present near the joints and mechanical pressure points in FD patients.[2] Development of a hoarse voice, progressive arthritis with joint deformities, and neurological and visceral involvement are also common.[3] Skin lesions characterized by extensive fibrosis in reticular dermis with hyalinized collagen have been described.[4] Accumulation of storage-laden macrophages is commonly noted at the tissue level, and many cell types including fibroblasts, hepatocytes, Schwann cells, and endothelial cells accumulate storage material into the typical "Farber" or "Zebra" bodies seen by electron microscopy.[4,5]

We previously developed *Asah1^{tm1Medin}*, a mouse model of FD (*Asah1^{P361R/P361R}*).[6] This mouse is homozygous for a C to G point mutation in *Asah1* resulting in the replacement of proline with arginine at position 361 (P361R).[6] This mutation corresponds to a mutation previously identified in patients with FD.[6] These mice have a 129S6/SvEvTac x CD-1 genetic background and have been inbred in our lab for over 20 generations. This mouse model recapitulates symptoms described in many FD patients. Manifestations include central nervous system,[7] chronic lung,[8] hepatic,[9] and ocular abnormalities.[10] The most prominent features of our murine model are systematic accumulation of ceramides and foamy macrophages in organs that are a hallmark of FD, a shortened life span, decreased body weight, hepatosplenomegaly, and stiffness of the skin with reduced fat pads throughout the body.

In this work, we analyzed the skin of *Asah1^{P361R/P361R}* mice. We show altered lipid and sphingolipid composition in FD mouse skin and a differential spectrum of ceramide species within individual skin cells—representing the main cell types found in each of the epidermis, dermis, and hypodermis. Biochemical, histological, and ultrastructural examination of *Asah1^{P361R/P361R}* mice revealed massive storage of nondegraded substrates affecting mainly the dermal reticular layer spreading to the connective tissue of the hypodermis. Significant inflammation, a reduction of AT, and impaired adipogenesis of adipose-derived stem/stromal cells (ASC) isolated from the stromal vascular fraction (SVF) of white AT was also observed.

2 | MATERIALS AND METHODS

2.1 | Mouse procedures

Mice were housed in pathogen-free conditions and all procedures were approved by the MCW Institutional Animal Care and Use Committee. Genotyping was performed as previously reported.[6] All mice were euthanized by exposure to CO_2 or Isoflurane. Mice were sprayed with 70% ethanol and shaved at the back of the neck. Neck skin samples were collected for MS/MS and western blot analysis and stored at $-80°C$. Skin samples for histology, immunohistochemistry or ultrastructural study were fixed by immersion in 10% phosphate-buffered formalin or 4% paraformaldehyde, respectively, for 24–48 h and stored at 4°C.

2.2 | Scruff measurement

The length of wild-type (WT), *Asah1^{+/P361R}* heterozygous, and *Asah1^{P361R/P361R}* homozygous mouse neck scruff was measured by millimeter caliper weekly from 3 to 9 weeks of age when *Asah1^{P361R/P361R}* mice die to disease progression.

2.3 | Skin histopathology and immunohistochemistry

Skin samples fixed in 10% phosphate-buffered formalin were trimmed, embedded in paraffin wax, and sectioned at 4 μm. Skin sections were stained with hematoxylin and eosin. The following primary antibodies were used for skin immunohistochemistry: rat antimouse Mac-2 (Galectin-3 clone M3/38, Cedarlane) and rabbit Cathepsin D (CatD; Abcam, Cambridge, Massachusetts). The following secondary antibodies were used to detect primary antibodies: biotinylated rabbit antirat Immunoglobulin G (IgG) (Vector laboratories, Burlingame, California) and biotinylated goat antirabbit IgG (Vector Laboratories). DAB kit (Vector Laboratories) was used for secondary detection according to the manufacturer's instructions. Slides were scanned on the Aperio AT2 histology slide scanner (Leica Biosystems, Buffalo Grove, Illinois) or NanoZoomer 2.0-HT histology slide scanner (Hamamatsu Photonics, Ichinocho, Japan). Scanned micrographs were analyzed with Aperio ImageScope analysis software (Leica Biosystems).

For Oil Red O staining, skin samples fixed in 10% phosphate-buffered formalin were washed with phosphate-buffered saline (PBS), treated with 10%, 20%, and 30% sucrose in PBS for 10 min in each solution, covered

with Cryomatrix (Thermo Fisher Scientific, Waltham, Massachusetts) and lowered into an isopentane (Sigma-Aldrich, St. Louis, Missouri) mold cooled in liquid nitrogen. Upon solidification, the samples were stored at −80°C until ready to cut. Skin sections were stained with Oil Red O (Sigma-Aldrich) by standard techniques.

2.4 | Electron microscopy

Skin samples from 5-week to 9-week-old $Asah1^{P361R/P361R}$ and WT control mice were processed for electron microscopy as detailed previously.[8] Ultrathin sections were evaluated using the JEOL 1400+ (JEOL, Tokyo, Japan) transmission electron microscope equipped with Olympus Veleta CCD camera and Radius Software (EMSIS GmbH, Munster, Germany).

2.5 | Western blot analysis

The skin tissue samples were homogenized in pH 8 RIPA buffer (50 mM Tris, 150 mM NaCl, 1% Triton X-100, 1% sodium deoxycholate, 0.1% sodium dodecyl sulfate (SDS), and 1 mM EDTA) containing HALT Protease and Phosphatase Inhibitor Cocktail (Thermo Fisher Scientific). Samples were homogenized using a Bullet Blender Storm 24 (Next Advance, Troy, New York) tissue homogenizer with 0.5 mm zirconium oxide beads (Next Advance). Lysates were centrifuged (19 000 g, 10 min, 4°C) to remove impurities and stored at −80°C. Protein concentration was determined using a BCA assay (Thermo Fisher Scientific). In total, 20 μg of each sample was separated using 10% SDS-gel electrophoresis and subsequently transferred to polyvinylidene fluoride (PVDF) membrane (Millipore, Billerica, Massachusetts). Primary antibodies used are summarized in Table S1. HRP-conjugated antirabbit IgG (cn: A6154, Sigma-Aldrich) was used as secondary antibody. Immunoreactivity was visualized with enhanced chemiluminescence substrate (Thermo Scientific) on a ChemiDoc MP (Bio-Rad Laboratories, Inc, Des Plaines, Illinois). Band densitometry was quantified using ImageJ software v.1.51 (NIH). Total amount of detected proteins were normalized to β-actin loading controls (cn: a3854, Sigma-Aldrich). Detected proteins from WT and $Asah1^{P361R/P361R}$ mice were expressed relative to normalized proteins from WT mice. Skin cells cultured in 6-well plates were washed twice with PBS and 75 μl of cold RIPA buffer (Thermo Fisher Scientific) was added for lysis on ice. Cells were scraped, collected into Eppendorf tubes, and centrifuged (14 000 g for 15 min) to remove debris. Clear homogenates were used for protein determination and western blot analysis as described above.

2.6 | Mouse skin lipid extraction

To obtain a homogenates of the required dilution, 1 ml of MilliQ water was added to 100 μg of tissues. Tissue processing consisted of mechanical homogenization in an Ultra-Turrax (Miccra D-9, MICCRA GmbH, Heitersheim, Germany) followed by ultrasonic homogenization in a cup horn (Digital Sonifier Model 450, BRANSON Ultrasonics Corporation, Danbury, Connecticut) and finally lyophilization (Christ L-1, B-Braun Biotech International GmbH, Melsungen, Hessen, Germany) of the homogenized samples. Lyophilized tissues were reconstituted in 1 ml of MilliQ water and mechanical and ultrasonic steps were repeated.

Protein content in homogenates was measured by the method of Hartree.[11] Lipid extraction was performed by the method of Natomi.[12] Briefly, 250 μl of homogenates were repeatedly extracted with chloroform:methanol:water mixtures of increasing polarity from 2:1:0.1 (vol/vol/vol), 1:1:0.1 (vol/vol/vol), and 1:2:0.1 (vol/vol/vol). Liquid phases were separated from protein residues after application of each mixture and combined. The extracts were dried under a stream of nitrogen and reconstituted in chloroform: methanol (2:1; vol/vol) to reach the final protein concentration of 1 μg/μl and stored at −20° C prior to processing for lipid analysis. Lipids were analyzed on AB/MDS SCIEX API4000 triple quadrupole tandem mass spectrometer with electrospray ionization (ESI; Applied Biosystems, Waltham, Massachusetts) coupled to an Agilent UPLC Infinity 1290 system equipped with an autosampler (Agilent Technologies, Santa Clara, California).

Lipid extracts for analysis of gangliosides and sulfatides were prepared from a 40 μg protein aliquot of homogenates; cholesterol and esters of cholesterol were prepared from a 10 μg protein aliquot as described previously.[13,14] Samples for analysis of other lipids were prepared from 5 μg protein aliquots. All samples were measured in technical replicates and average values were calculated for each sample. Lipids were analyzed by two approaches. ceramide (Cer), monohexosylceramides (MHC), dihexosylceramides (DHC), globotriaosylceramide (Gb3Cer), globotetraosylceramide (Gb4Cer), sphingomyelin (SM), sulfatide (SGalCer), monosialogangliosides 1 (GM1), GM2, and GM3 were analyzed by flow injection ESI tandem mass spectrometry (FIA-ESI-MS/MS) using methanol as the mobile phase.[15] A different approach combining ESI tandem mass spectrometry with liquid chromatography (LC-ESI-MS/MS) was used for the analysis of cholesterol (Chol), esters of cholesterol (CholE),[13] sphingosine (SPH), lysosphingomyeline, and lyso-sphingomyeline-509.[16] Both FIA-ESI-MS/MS and LC-ESI-MS/MS utilized single reaction monitoring with optimized instrument settings to measure each lipid class based on their specific fragments as previously published.[15] Results

were analyzed using Analyst 1.6.3 software (AB Sciex Pte. Ltd, Singapore). The concentration of these lipids was calculated according to previously published methods by single point calibration with a known lipid concentration in external calibration standard corrected by the signal ratio toward internal standard (IST).[15] Final concentrations of each lipid class or molecular species were expressed as pmol of analyzed lipid per mg of protein. Molecular species (isoform) profiles were calculated using measured signals of individual molecules. Final concentrations were expressed as pmol of lipids per mg of protein.

2.7 | Establishment of primary skin cell cultures

2.7.1 | Isolation of ASC from white AT

White AT was collected from 4-week to 5-week-old $Asah1^{P361R/P361R}$ and WT mice as previously described.[17,18] Briefly, the mice were euthanized by exposure to isoflurane followed by cervical dislocation. Subcutaneous and visceral white AT were collected and placed in sterile PBS with 1% bovine serum albumin (BSA) and transported on ice into a laminar flow hood. ATs were thinly sliced with a scalpel and placed into Dulbecco's Modified Eagle Medium (DMEM)/F12 media (Thermo Fisher Scientific) supplemented with Dispase (Sigma-Aldrich) at 26 Wunsch units/ml in PBS. The samples were incubated at 37°C for 30 min in a water bath for tissue digestion. Once digested, the solutions were filtered through a sterile 40 μm filter into a sterile 50 ml conical tube and centrifuged at 400 g at room temperature for 5 min. Supernatants were discarded, and the cell pellets were resuspended in DMEM/F12 media supplemented with 1× Pen/Strep (Thermo Scientific) and 10% fetal bovine serum (FBS; Thermo Scientific) and cultured in a 37°C humidified 5% CO$_2$ incubator. Unattached cells were removed 24 h later and media changes were performed every other day. ASCs were passaged with 0.25% Trypsin/EDTA solution (Thermo Scientific) when the cells reached 90% confluency.

2.7.2 | Generation of primary fibroblast cultures from mouse ears

The mice were euthanized by CO$_2$ nacrosis. Mouse ears from 4-week to 5-week-old WT and $Asah1^{P361R/P361R}$ mice were sprayed with 70% ethanol, dried, cutoff, placed into a 1.5 ml microfuge tube with cold sterile PBS on ice and transferred into a laminar flow hood. The ears were then washed with PBS in a 10 cm culture dish, dried on tissue paper, and cut into 3 mm or smaller pieces with a scalpel. Ear tissue from each mouse was transferred into one well of a 6-well plate in 3 ml of DMEM media (Thermo Scientific) supplemented with Liberase (Roche Diagnostics) at 0.14 Wunsch unit/ml for 2 h in a 37°C humidified 5% CO$_2$ incubator. Once digested, 2 ml of complete DMEM media (supplemented with 1× Pen/Strep and 10% FBS) was added to each well and the tissue solutions were transferred into 15 ml conical tubes and centrifuged at 400 g at room temperature for 5 min. The supernatants were discarded, and the tissues were washed twice with 7 ml of complete DMEM media. Once washed, the tissues were resuspended in 5 ml of complete DMEM media and transferred into 25 cm^2 culture flasks and incubated in a 37°C humidified 5% CO$_2$ incubator. The cells started to migrate from the ear tissue by the second or third day in culture. Ear tissues were removed by the sixth day in culture. Cell cultures of 70% confluency were passaged using 0.25% Trypsin/EDTA solution.

2.7.3 | Generation of primary keratinocyte cultures from mouse tail skins

Cultures of primary keratinocytes (KC) were established using a modified previously published protocol.[19] Briefly, the tails of euthanized 4-week to 5-week-old WT and $Asah1^{P361R/P361R}$ mice were cut off at the base of the tail, placed into 15 ml conical tubes containing sterile PBS on ice and transferred into a laminar flow hood. The tail skin was cut from the base to the tip of the tail and gently peeled off the bone. Peeled skins were washed with sterile PBS and placed into a 2 ml tube containing 4 mg/ml Liberase (Roche Diagnostics) in complete CnT-07 medium (CELLnTEC, Bern, Switzerland) and incubated overnight in a 4°C refrigerator. The next day, the skin tissues were transferred on a Petri dish in the laminar flow hood and carefully washed twice with sterile PBS. The epidermis was carefully detached from the dermis by forceps. Stretched epidermis without folds was then transferred into 0.5 ml of 0.25 Trypsin/EDTA solution in new Petri dishes and incubated for 20 min at room temperature. In total, 2 ml of KC growth medium was added, and the epidermis was vigorously rubbed back and forth to release single cells from the epidermal sheets. The epidermis was washed twice with an additional 2 ml of medium and the cell suspension was collected into a 15 ml conical tube. The cells were filtered and centrifuged at 200 g at room temperature for 5 min. The supernatant was discarded, and the cells were resuspended in 4 ml of KC growth medium. Immature KC were divided into 2 wells of a 6-well culture plate and cultured in a 37°C humidified 5% CO$_2$ incubator. Fresh media was replenished every other day. Finally, 0.06 mM CaCl$_2$ (Sigma-Aldrich) in PBS was added to the culture media for 5 days to induce terminal differentiation of KC.

2.8 | Differentiation of fibroblasts and preadipocytes into mature adipocytes

ASC isolated from white AT and fibroblasts established from the ears were used for differentiation into adipocytes as described previously.[17,18] Cells were counted using Trypan Blue (Thermo Scientific) exclusion with the Countess II FL automated cell counter (Life Technologies, Carlsbad, California) and 200 000 ASC or fibroblast cells were seeded into one well of 6-well plate and left to grow for 3–4 days to reach 90% confluency. The cell lines were prepared in quadruplicates (with $n = 3$ per genotype). When the cells reached 90% confluency, the media was collected for cytokine release by enzyme-linked immonosorbent assays (ELISAs) and the first two singlets of cells were harvested for western blot and MS/MS analysis. The second two singlets of cells were used for adipocyte differentiation by addition of DMEM/F12 media (Thermo Scientific) supplemented with 1× Pen/Strep, 10% FBS and differentiation factors: 0.5 μM methylisobutylxanthine, 0.2 nM insulin, 5 nM rosiglitazone, and 1 nM dexamethasone (all from Sigma-Aldrich) for 5 days. The medium was replaced with fresh media without differentiation factors on the fifth day and the cell cultures were left to grow for an additional 2 days. Media from ASC-derived adipocytes (ASC-A) and fibroblast-derived adipocytes (Fibro-A) was collected for cytokine release ELISAs at 7 days post-differentiation. The cells for western blot and MS/MS analysis were harvested 14 days post-differentiation.

2.9 | Oil Red O stain of neutral lipids in adipocytes

ASC-A and Fibro-A were prepared as described above. On the seventh day of differentiation, the cells were washed with PBS (2 × 5 min), fixed in 4% PFA in PBS for 15 min, and washed with PBS (2 × 5 min). A working solution of Oil Red O was prepared by diluting 6 ml of 0.5% Oil Red O isopropanol solution (Sigma-Aldrich) in 4 ml of distilled water. In total, 1 ml of freshly prepared working Oil Red O solution was added to each well of a 6-well plate containing the skin cells and incubated at room temperature for 30 min. After incubation, the Oil Red O solution was discarded, and the cells were washed in PBS (2 × 5 min) followed by distilled water (1 × 5 min). The cells were maintained in distilled water until imaging using a Nicon Ellipse TS100 microscope with ELWD 0.3/0D75 camera (Nicon Inc, Tokyo, Japan).

2.10 | Skin cell line lipid extraction

Cells were processed as previously described.[20] Briefly, cell pellets were reconstituted in 250 μl of MilliQ water and homogenized by ultrasound using a Digital Sonifier Model 450 (Branson Ultrasonics Corporation, Danbury, Connecticut). Protein concentration was analyzed by Bradford assay and a modified Folch method was used for lipid extraction.[20] Briefly, lipids were extracted from 200 μl homogenates after addition of 800 μl of chloroform:methanol (2:1; vol/vol). Upper and lower liquid phases, were separated from the protein precipitate, combined, and evaporated under a stream of nitrogen. Dry lipid extracts were reconstituted in chloroform:methanol (2:1; vol/vol) prior to processing for lipid analysis as described above (mass spectrometry of lipids).

2.11 | Cytokine analysis and ELISA

The media collected from cultured ASC, fibroblasts, ASC-A, and Fibro-A was centrifuged at 5000 g for 5 min and the supernatants were stored at −80°C until further use. Mouse tumor necrosis factor alpha (TNF-α) (cn: 430904), mouse interleukin 6 (IL-6) (cn: 431304), and mouse monocyte chemotactic protein-1 (MCP-1; cn: 432701) ELISA kits (all from Biolegend, San Diego, California) were used to detect concentration of the appropriate cytokines in media in accordance with the manufacturer's instructions.

For cytokine release in SVF isolated from AT, the AT was collected from 4-week to 5-week-old WT and $Asah1^{P361R/P361R}$ mice and processed as described above (isolation of ASCs from white AT) with the exception that following Dispase digestion the cells were filtered through a sterile 100 μm filter. After centrifugation, the cells were resuspended in DMEM/F12 media supplemented with 1× Pen/Strep and 10% FBS (Thermo Fisher), counted and plated at the same concentration, and cultured for 4 days in a 37°C humidified 5% CO_2 incubator without a media change. Media was collected on Day 4, centrifuged at 5000 g for 5 min, and supernatants were stored at −80°C until further use.

2.12 | Flow cytometry

For detection of immune cells in SVF isolated from AT of WT and $Asah1^{P361R/P361R}$ mice, the cells were prepared as described above for cytokine analysis. After filtration of the cells, they were washed with Dulbecco's PBS containing 0.5% BSA and 0.05% sodium azide. After washing, the

cells were stained with fluorescence-conjugated antibodies FITC antimouse CD11b (cn: 101205 Biolegend) and PE anti-mouse CD14 (cn: 150105, Biolegend) for 30 min at 4°C, washed and analyzed using a LSR II flow cytometer (BD Bioscience, San Jose, California) and FlowJo software v10 (Becton Dickinson and Company, Ashland, Oregon).

2.13 | Immunocytochemistry of differentiated adipocytes

ASC-A and Fibro-A were fixed in 4% PFA in PBS for 15 min, permeabilized with 0.2% Triton-X100 in PBS for 5 min, and blocked in 10% FBS in PBS for 1 h, all at room temperature as previously described.[21] The cells were incubated overnight at 4°C with primary antibodies CatD (cn: ab75852, Abcam) and mouse Adiponectin (cn: BS8216211, MyBioSource, San Diego, California) diluted in blocking buffer. Later 24 h, the samples were washed with PBS (5 × 5 min) and the cells were labeled with Alexa Fluor 488 goat antimouse and Alexa Fluor 594 goat antirabbit fluorescence-conjugated secondary antibodies (both from Thermo Scientific) for 1 h at 37°C. The cells were then washed with PBS (5 × 5 min) and mounted using Vectashield mounting media (Vector Laboratories, Burlingame, California) containing 4′,6-diamidino-2-phenylindole (DAPI) to counterstain cell nuclei. Images were captured using AxioImager (Carl Zeiss, Germany) upright microscope using 20× or 40× Plan-apo-lenses. GFP/Alexa 488 was imaged with Filter set 37 (EX-BP 450/50, BS-FT480, and Em-BP 510/50), RFP/Alexa 594 was imaged using Filter set 20 (EX-BP 546/12, BS-FT560, and Em-BP 575–640) and DAPI was captured with Filter set 34 (EX-BP 390/22, BS-FT420, Em-BP 460/50). Axiovision software/Axiocam HRm 1.4 MP color camera (Carl Zeiss, Germany) was used to record images with fixed exposure time for each fluorophore based on the positive control.

3 | RESULTS

3.1 | Histopathology and structural changes throughout the skin with reduced AT in $Asah1^{P361R/P361R}$ mice

$Asah1^{P361R/P361R}$ mice display stiff neck skin as they age. While measurements of WT ($Asah1^{+/+}$) and $Asah1^{P361R/+}$ heterozygous mouse nape skin length (scruff) assessed by caliper measurement increased over time, $Asah1^{P361R/P361R}$ mouse scruff plateaued over the first month of age and was found to be statistically reduced by 3 weeks of age (Figure 1A). No differences were noted between male and female $Asah1^{P361R/P361R}$ mouse scruff measurements.

We next evaluated skin tissue from WT and $Asah1^{P361R/P361R}$ mice for histological differences. The major abnormality seen in the skin of $Asah1^{P361R/P361R}$ mice by 5 weeks of age was the accumulation and local clustering of cells with foamy cytoplasm in the dermis and hypodermis (Figure 1B). This was substantially increased in skin samples from 9-week-old $Asah1^{P361R/P361R}$ animals and was associated with near complete loss of hypodermal AT (Figure 1B). Oil Red O-stained frozen sections showed greatly reduced neutral triglycerides and lipid droplets of adipocytes from samples of 9-week-old $Asah1^{P361R/P361R}$ mice compared with those from animals 5 weeks of age (Figure S1A). The panniculus carnosus muscle was also thinned and atrophic in $Asah1^{P361R/P361R}$ mice. Last, the epidermal stratum corneum was thicker in $Asah1^{P361R/P361R}$ compared with WT mice (Figure 1B).

We next assessed the abnormal dermal and hypodermal foamy cells by staining with anti-Mac2 antibody. The highest local accumulation of Mac-2+ cells was seen in tissues from 9-week-old $Asah1^{P361R/P361R}$ animals at the interface of the dermis and panniculus carnosus muscle. At that age, these cells virtually replaced the hypodermal AT (Figure 1C). $Asah1^{P361R/P361R}$ mice also displayed increased lysosomal aspartyl protease CatD at 9 weeks of age at the interface of the dermis and hypodermis (Figure S1B).

Western blots were conducted on WT and $Asah1^{P361R/P361R}$ mouse skin lysates revealed increased lysosomal CatD and autophagy marker LC3-II (Figure S1C,D).

Ultrastructural analyses showed lysosomal storage abnormalities similar to those previously reported in a range of tissues and cell types from $Asah1^{P361R/P361R}$ mice.[7–9] The most affected cell types were the dermal and hypodermal macrophages (Figure 2A). Storage could be detected in the epidermal epithelia (Figure 2B), basal cells of outer hair root shafts (not shown), and basal cells of the sebaceous epithelium (Figure 2C). Typical spindle-shaped storage bodies were found in the Schwann cell's cytoplasm of small peripheral nerves (Figure 2D). Storage abnormalities in the endothelial cells and cells of the vascular wall(s) corresponded to the changes reported in other tissues.[7–9]

3.2 | Altered sphingolipid profile in the skin of $Asah1^{P361R/P361R}$ mice

Lipid and sphingolipid species were quantified in skin extracts from 5-week and 9-week-old WT and $Asah1^{P361R/P361R}$ mice by FIA-ESI-MS/MS or LC-ESI-MS/MS. Skin from $Asah1^{P361R/P361R}$ mice displayed pronounced accumulation of total Cer, SPH, free cholesterol (Chol), and sphingomyelin (SM) compared with control mice (Figure 3A). Neutral glycosphingolipids (GSL), representing important products in the biosynthesis of

FIGURE 1 $Asah1^{P361R/P361R}$ mice display decreased neck skin scruff and structural skin abnormalities. Decreased neck scruff caliper measurements of $Asah1^{P361R/P361R}$ mice in comparison to wild-type (WT) and $Asah1^{P361R/+}$ heterozygous mice (A). Hematoxylin and eosin (H&E) staining of 5-week-old $Asah1^{P361R/P361R}$ and 9-week-old $Asah1^{P361R/P361R}$ and WT skin sections. Epidermis (E), dermis (D), hypodermal adipose tissue (HAT) and panniculus carnosus muscle (PCM) are indicated (B). Macrophage marker Mac-2 staining in 5-week-old $Asah1^{P361R/P361R}$ and 9-week-old $Asah1^{P361R/P361R}$ and WT skin sections (C). Scale bars (B,C) = 100 μm. Thickness of adipose tissue layers and Mac-2 quantification in 5-week and 9-week-old WT and $Asah1^{P361R/P361R}$ mice were analyzed by one-way analysis of variance (ANOVA), $*p < 0.05$, $**p < 0.01$, $****p < 0.0001$, $\pm$SD (n = 3 males, 3 females per group; B,C). FD, Farber disease
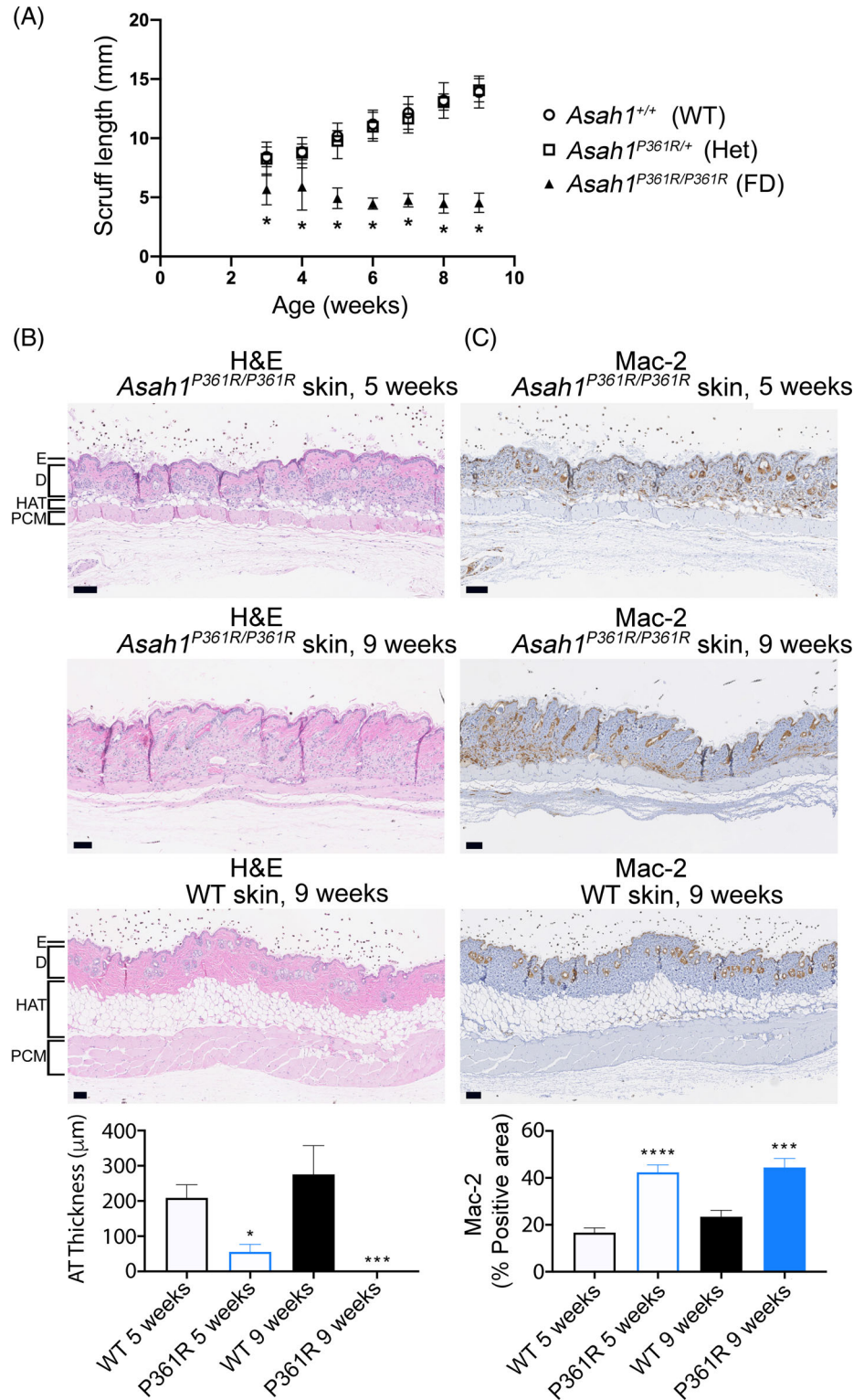
more complex GSL from ceramide, including monohexosylceramides (MHC; glucosylceramide and galactosylceramide), dihexosylceramides (DHC), Gb3Cer, and Gb4cer, were significantly increased in $Asah1^{P361R/P361R}$ mice compared with controls (Figure 3A). Ganglioside GM1 was elevated (Figure 3A), but gangliosides GM2 and GM3 were normal (data not shown). SPH was significantly elevated (Figure 3A), and a trend toward increased dihydro-SPH was seen in tissues from 9-week-old $Asah1^{P361R/P361R}$ mice (data not shown).

Many individual Cer species were significantly increased in $Asah1^{P361R/P361R}$ mice (Figure 3B). Increases were seen in C16:0, C24.1, C22:0, C24:0, and C24:2 moieties; and in hydroxyl-Cer species including C22:0-OH, C22:1-OH, C24:0-
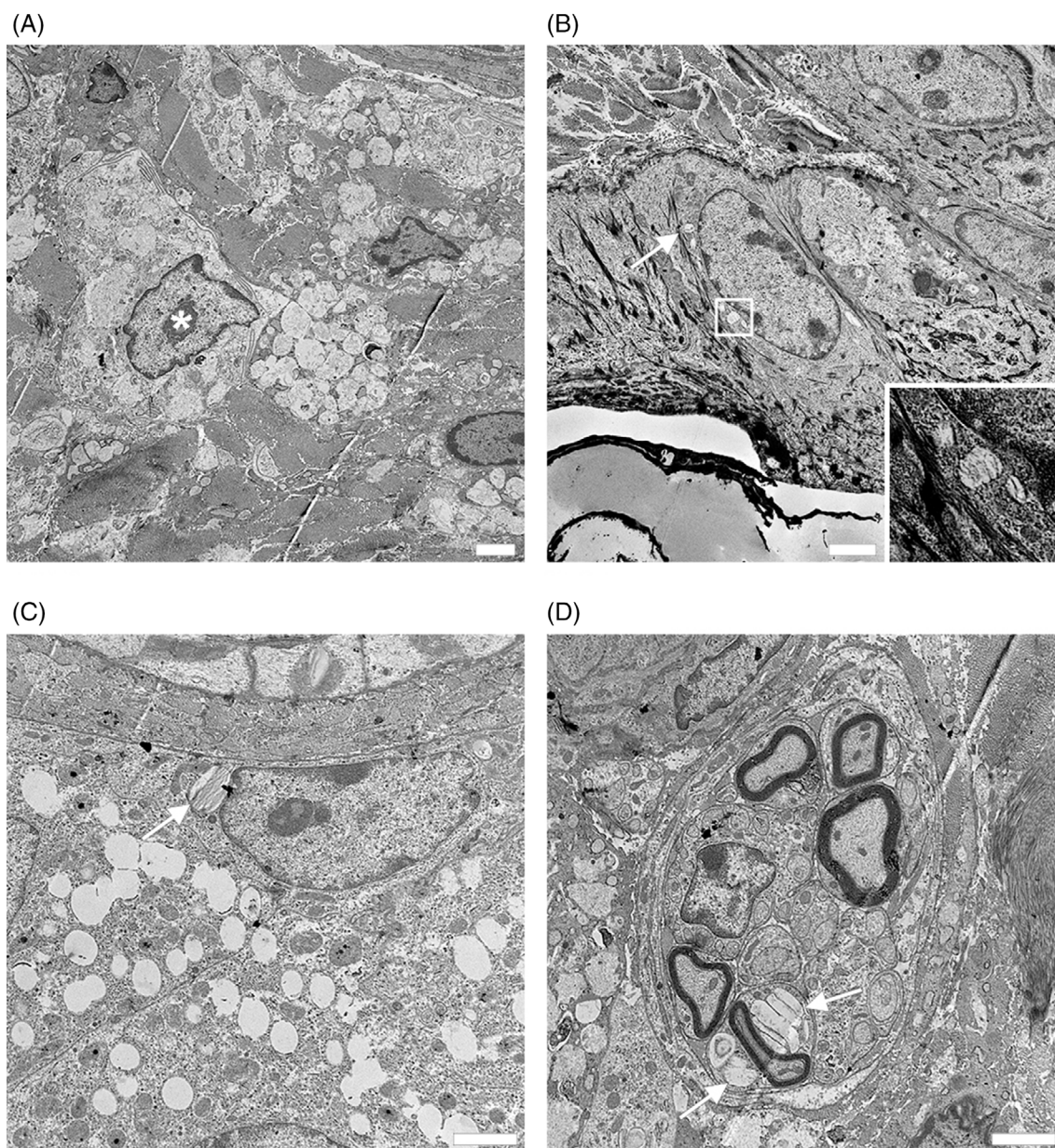
FIGURE 2 Ultrastructural analysis of skin in $Asah1^{P361R/P361R}$ mice. Electron microscopy conducted on skin samples from 9-week-old $Asah1^{P361R/P361R}$ mice. Dermal macrophages (nucleus of one highlighted by asterisk) with excess storage vacuoles (A); cytoplasm of epidermal epithelia (B); basal cells of sebaceous glands containing discrete storage vacuoles (arrows in C) and peripheral nerve Schwann cells with banana/spindle-shaped storage bodies (D). Scale bars = 2 μm

OH, C24:1-OH, C24:2-OH, and C26:0-OH. In contrast, no change was noted in C14:0, C20:0, or in Cer species containing longer fatty acid chains (Figure 3B). MHC species increases in the $Asah1^{P361R/P361R}$ skin extracts were similar to those of corresponding Cer species including C16:0, C18:0, C22:0, C24:0 and C24:1, C24:2, and C24.0-OH (Figure 3C). Total SM was increased in 9-week-old $Asah1^{P361R/P361R}$ mice, with C16:0, C20:0, C22:0, C24:1, and C24:2 being elevated (Figure 3D). C20:1-OH and C22:1-OH were the only two hydroxylated species of SM increased (Figure 3D).

3.3 | Activation of inflammatory IL-6/ JAK/signal transducer and activator of transcription 3 and noncanonical NF-κB signaling pathways in the skin of $Asah1^{P361R/P361R}$ mice

STAT3 (signal transducer and activator of transcription 3), NF-κB (nuclear factor kappa-light-chain-enhancer of activated B cells), and MAPK (mitogen-activated protein kinase) are common signaling pathways involved
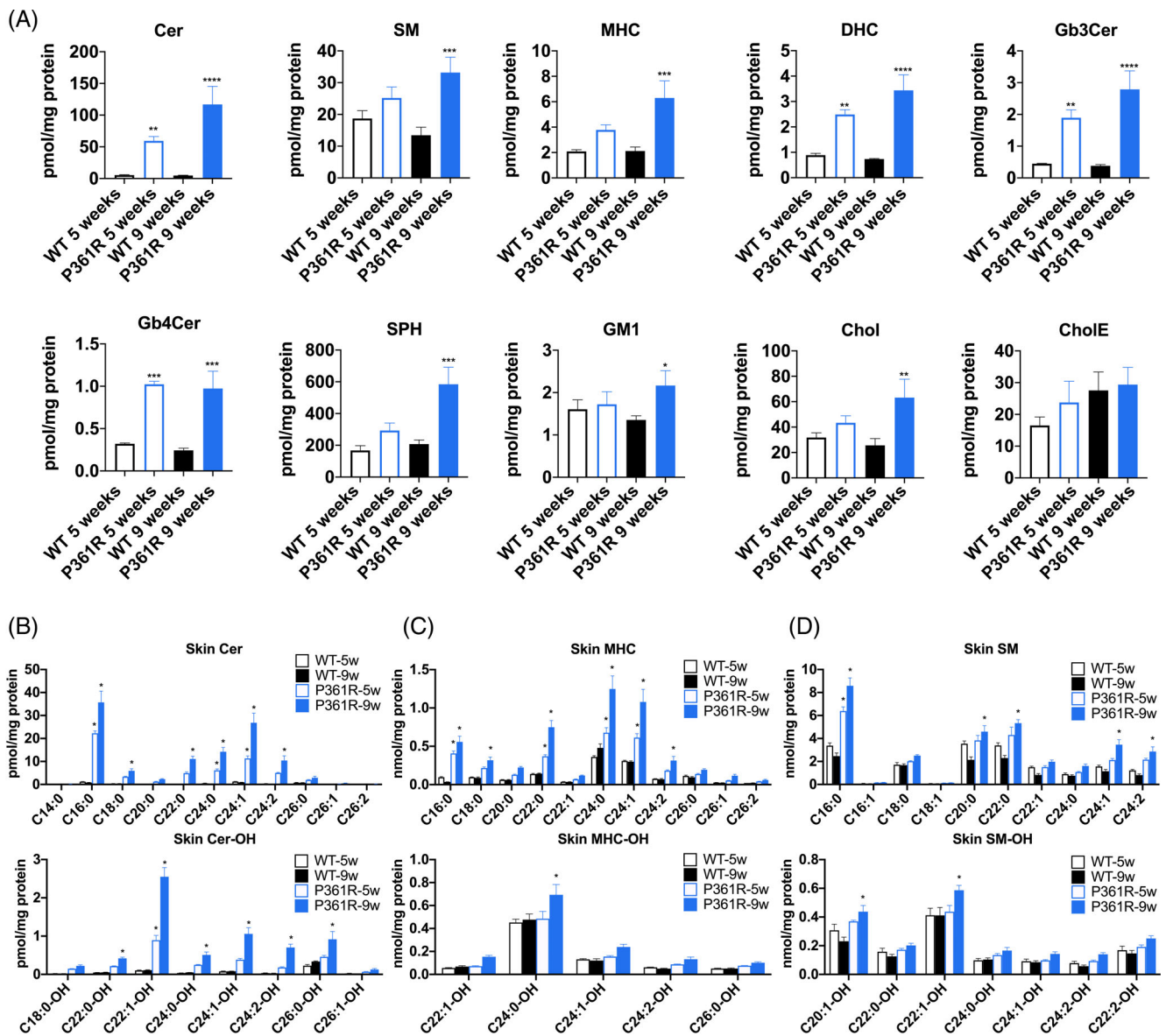
FIGURE 3 Abnormal sphingolipid accumulation in the skin of $Asah1^{P361R/P361R}$ mice. Skin lipid and sphingolipid levels were quantified by tandem flow injection electrospray ionization tandem mass spectrometry or liquid chromatography electrospray ionization tandem mass spectrometry in skin extracts from 5- and 9-week-old wild-type (WT) and $Asah1^{P361R/P361R}$ mice. Quantification of total ceramide (Cer), sphingomyelin (SM), monohexosylceramide (MHC, including glucosylceramide and galactosylceramide), dihexosylceramides (DHC), globotriaosylceramide (Gb3Cer), globotetraosylceramide (Gb4cer), sphingosine (SPH), monosialoganglioside 1 (GM1), cholesterol (Chol), and cholesterol esters (CE) in skin lysates from WT and $Asah1^{P361R/P361R}$ mice (A). Statistical analyses of (A) by one-way ANOVA, $*p < 0.05$, $**p < 0.01$, $***p < 0.001$, $****p < 0.0001$, $\pm$SD. Quantification of Cer and Cer-OH species (B); MHC and MHC-OH species (C); and SM and SM-OH species (D) differing in fatty acid chains in skin extracts from WT and $Asah1^{P361R/P361R}$ mice. Statistical analyses of (B–D) by two-way analysis of variance (ANOVA) with Bonferroni's multiple comparisons test to corresponding WT, $*p < 0.05$, $\pm$SD ($n = 3$ mice per group)

in skin inflammation.[22] Skin tissue lysates from 9-week-old WT and $Asah1^{P361R/P361R}$ mice were analyzed by western blot (Figure 4). While total STAT3, NF-κB, and MAPK levels remained similar, increased phosphorylation of STAT3 and NF-κB compared with WT was detected in all $Asah1^{P361R/P361R}$ lysates (Figure 4A–C). MAPK expression was found to be normal (Figure 4A,D). Activation of STAT3 is part of the IL-6/Jak (Janus kinase)/STAT3 signaling pathway. In

accordance with this, we detected increased phosphorylation of JAK in skin lysates from $Asah1^{P361R/P361R}$ mice (Figure 4E,H). To elucidate if the IL-6 receptor is involved in the activation of STAT3, we isolated total cells from AT of 4-week to 5-week-old WT and $Asah1^{P361R/P361R}$ mice and monitored cytokine release by ELISAs (Figure 4K–M). We chose 4-week to 5-week-old mice as the fat pads across their bodies have become negligible in 9-week-old $Asah1^{P361R/P361R}$ mice. IL-6 was
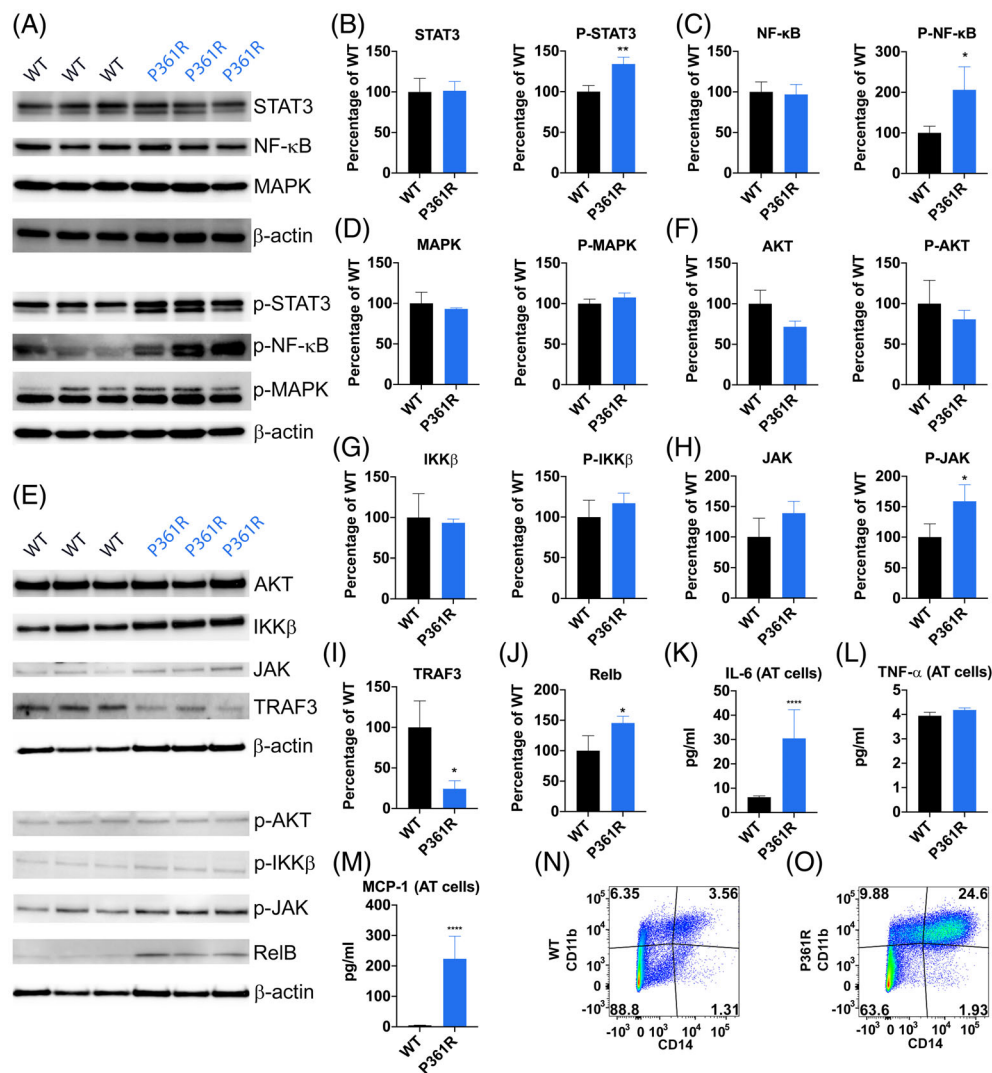
FIGURE 4 Activation of IL-6/JAK/signal transducer and activator of transcription 3 (STAT3) and noncanonical NF-κB inflammatory signaling pathways in the skin of $Asah1^{P361R/P361R}$ mice. Representative immunoblots of total and phosphorylated inflammatory proteins STAT3, NF-κB, and mitogen-activated protein kinase (MAPK) in tissue lysates from 9-week-old wild-type (WT) and $Asah1^{P361R/P361R}$ mice (A) and their quantification relative to WT mice (B–D). Representative immunoblots of total TNF receptor-associated protein 3 (TRAF3), RelB, and total and phosphorylated proteins involved in inflammatory pathways Protein kinase B (AKT), IκB kinase(IKK)β, and JAK in tissue lysates from 9-week-old WT and $Asah1^{P361R/P361R}$ mice (E) and their quantification relative to WT mice (F–J). Cytokines IL-6 (K), TNF-α (L), and monocyte chemotactic protein-1 (MCP-1; M) in media collected from WT and $Asah1^{P361R/P361R}$ mouse adipose tissue (AT) cell cultures analyzed by ELISA. Cd11b and CD14 assessed in WT and $Asah1^{P361R/P361R}$ mouse AT cell cultures analyzed by flow cytometry (N,O). Statistical analyses by Student's t-test, *$p < 0.05$, **$p < 0.01$, ****$p < 0.0001$, ±SD ($n = 3$ mice per group)

significantly increased in media from $Asah1^{P361R/P361R}$ adipose cells compared with controls (Figure 4K), supporting a role for the IL-6/JAK/STAT3 pathway in FD inflammatory processes. We also detected a significant increase in MCP-1 in the $Asah1^{P361R/P361R}$ adipose cell culture media (Figure 4M), which corresponds with our previously reported data.[6] To elucidate what kind of immune cell types could be contributing to increased IL-6/MCP-1 release in these AT cultures from $Asah1^{P361R/P361R}$ mice, we investigated cells isolated from AT of WT and $Asah1^{P361R/P361R}$ mice by flow cytometry. We detected

increased CD11b+/CD14+ cells in these AT cultures from $Asah1^{P361R/P361R}$ mice compared with WT (Figure 4N,O) suggesting an increased presence of the monocyte/macrophage lineage.

Activation of the NF-κB inflammatory pathway occurs through two major signaling schemas: the canonical (classical) and noncanonical (alternative) pathways. Classical NF-κB signaling is controlled by IκB kinase (IKK) and Protein kinase B (AKT) that can be activated by TNF-α binding the TNF receptor.[23] Although increased phosphorylation of NF-κB in skin homogenates

from $Asah1^{P361R/P361R}$ mice was noted, changes in phosphorylated IKK and AKT proteins was not observed (Figure 4F,G). TNF-α expression was similar to WT samples suggesting that the classical pathway was not activated in $Asah1^{P361R/P361R}$ mice (Figure 4L). TNF receptor-associated protein 3 (TRAF3) has been described as a negative regulator of the noncanonical NF-κB signaling pathway. TRAF3 reduction has previously been associated with increased expression of several noncanonical NF-κB components including RelB, independent of TNF-α.[24] We detected significantly reduced expression of TRAF3 in $Asah1^{P361R/P361R}$ skin lysates along with increased activation of RelB—supporting activation of the noncanonical NF-κB pathway during inflammation in $Asah1^{P361R/P361R}$ mice (Figure 4I,J).

3.4 | Abnormalities of isolated epidermal keratinocytes and dermal fibroblasts from $Asah1^{P361R/P361R}$ mice

The skin is composed of two major layers: a superficial epidermis (consisting of keratinocytes) and the underlying dermis (predominantly fibroblasts).[25] Immature keratinocytes isolated from $Asah1^{P361R/P361R}$ tails did not show any morphological changes or altered proliferative capacity compared with those from WT mice. Addition of 0.2 mM $CaCl_2$ to aid keratinocyte maturation led to the formation of vacuoles or vacuole-like structures within $Asah1^{P361R/P361R}$ cells (Figure S2A). By western blot analyses, a trend toward increased CatD was noted in FD keratinocytes with and without $CaCl_2$ treatment. Trends
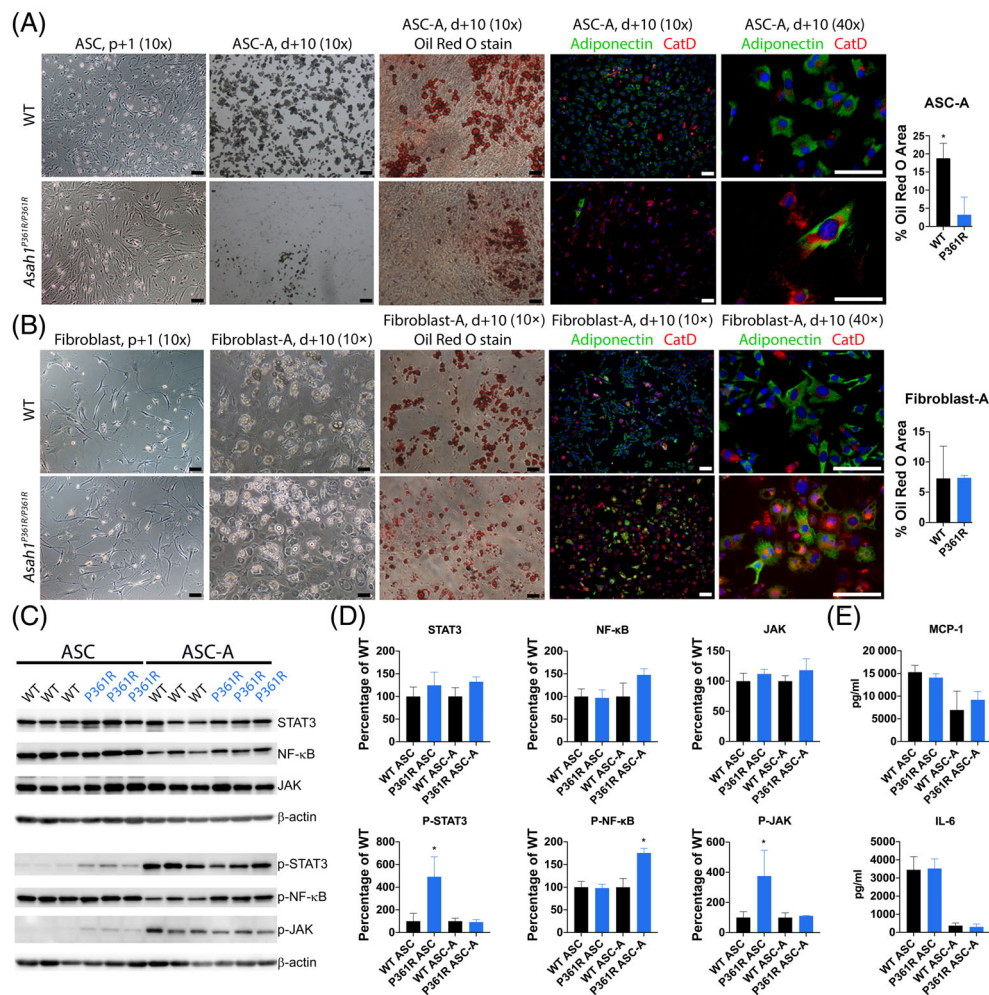
FIGURE 5 Impaired differentiation of $Asah1^{P361R/P361R}$ preadipocytes accompanied by activation of inflammatory pathways. Impaired adipogenesis of adipose-derived stem/stromal cell (ASC) from $Asah1^{P361R/P361R}$ mice visualized by reduced Oil Red O and adiponectin in mature $Asah1^{P361R/P361R}$ ASC-derived adipocytes (ASC-A) in comparison to wild-type (WT). $Asah1^{P361R/P361R}$ derived ASC-A showed decreased Oil Red O and CatD staining (A). $Asah1^{P361R/P361R}$ derived fibroblasts appeared to have similar Oil Red O and CatD staining and normal differentiation (B). Representative immunoblots of total and phosphorylated inflammatory proteins signal transducer and activator of transcription 3 (STAT3), NF-κB, and JAK in ASC and ASC-A homogenates from WT and $Asah1^{P361R/P361R}$ mice (C) and their quantification relative to WT mice (D). Monocyte chemotactic protein-1 (MCP-1) and IL-6 released in ASC and ASC-A cell culture media collected during adipogenesis assessed by ELISA (E; n = 3 mice per group). Scale bars (A,B) = 100 μm

toward increased expression of autophagy markers LC3-II, phospho-STAT3, and NF-κB in immature $Asah1^{P361R/P361R}$ keratinocytes were noted but not found to be statistically significant (Figure S2B).

Fibroblasts isolated from $Asah1^{P361R/P361R}$ ears showed reduced proliferation after their third cell passage compared with controls. After this time, we observed distinct formation of vacuole-like structures within $Asah1^{P361R/P361R}$ fibroblasts (Figure S2C) with the cells usually dying after several days in culture. WT fibroblasts did not form these structures and could be passaged without a decline in proliferative capacity. Similar to the FD keratinocytes, FD fibroblasts trended toward increasing CatD, LC3-II, and phosphorylated NF-κB levels but these changes were not found to be statistically significant (Figure S2C).

3.5 | Impaired differentiation of $Asah1^{P361R/P361R}$ preadipocytes isolated from AT was accompanied by activation of inflammatory pathways

Due to the observed AT reduction in $Asah1^{P361R/P361R}$ skin sections, we next investigated adipogenesis. We isolated ASCs from white subcutaneous AT of 4-week to 5-week-old WT and $Asah1^{P361R/P361R}$ mice. ASCs reside in the SVF of AT and can be isolated by extraction of the SVF from lipo-aspirates followed by enzyme digestion and centrifugation.[17] WT and $Asah1^{P361R/P361R}$ cells displayed similar morphology; but a reduced proliferation of $Asah1^{P361R/P361R}$ cells was noted after their third passage (not shown).

For adipogenic differentiation studies, confluent ASCs and fibroblasts were prepared as outlined in Figure S3A. We observed significantly reduced differentiation of $Asah1^{P361R/P361R}$ ASCs into adipocytes (ASC-A) in comparison with controls (Figure 5A) as well as with $Asah1^{P361R/P361R}$ fibroblasts (Figure 5B). These results were confirmed by reduced Oil Red O-stained lipid droplets and by reduced Adiponectin adipocyte marker staining (Figure 5A).

Interestingly, increased STAT3 and JAK phosphorylation was detected only in $Asah1^{P361R/P361R}$ ASCs compared with WT—while increased NF-κB phosphorylation was detected in $Asah1^{P361R/P361R}$ ASC-A (Figure 5C,D) suggesting activation of the IL-6/JAK/STAT3 signaling pathway at an earlier developmental stage. Analyses of cytokines released into the culture media during
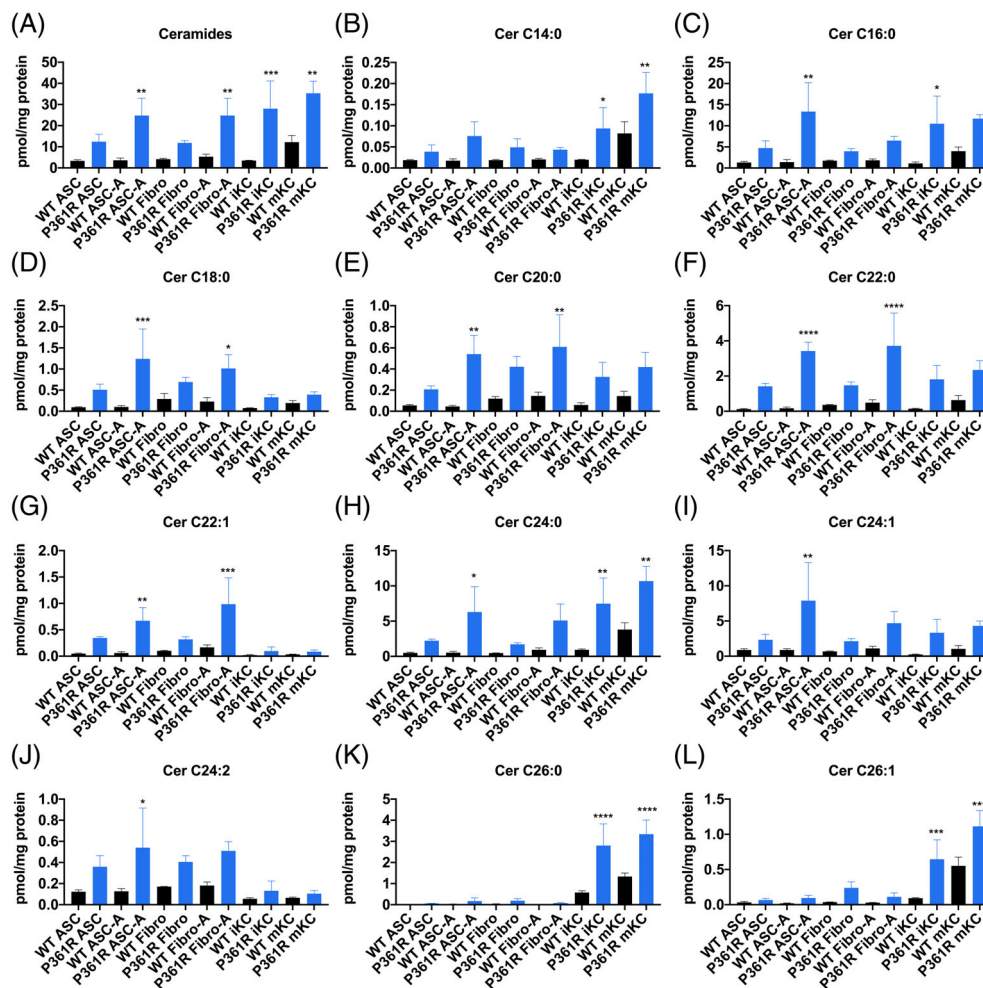
FIGURE 6 Abnormal accumulation of nonhydroxy-ceramide species in skin cells isolated from $Asah1^{P361R/P361R}$ mice. Total skin ceramide and its nonhydroxy species differing in fatty acid chains were quantified by flow injection electrospray ionization tandem mass spectrometry in extracts from immature keratinocytes (iKC), mature keratinocytes after addition of $CaCl_2$ (mKC), fibroblasts (Fibro), fibroblast-derived adipocytes (Fibro-A), adipose-derived stem/stromal cells (ASC), and ASC-derived adipocytes (ASC-A) from wild-type (WT) and $Asah1^{P361R/P361R}$ mice. Quantification of total skin ceramide (Cer) (A) and nonhydroxy ceramide species differing in fatty acyl chain length (B–L). Statistical analyses by one-way analysis of variance (ANOVA), $*p < 0.05$, $**p < 0.01$, $***p < 0.001$, $****p < 0.0001$, ±SD ($n = 3$ mice per group)

adipogenesis did not reveal significant changes to MCP-1 or IL-6 levels (Figure 5E), and that TNF-α expression was below the detection limit.

$Asah1^{P361R/P361R}$ ASC-A also showed increased accumulation of CatD compared with WT and to ASCs from both WT and $Asah1^{P361R/P361R}$ mice (Figure S3B,C). Autophagy marker LC3-II expression, as well as MAPK and AKT phosphorylation were normal (Figure S3D–H). None of these inflammatory proteins or cytokines were significantly increased in Fibro-A lysates or media (not shown).

3.6 | Abnormal ceramide accumulation in skin cells isolated from $Asah1^{P361R/P361R}$ mice

All skin lipid and sphingolipid species in extracts of ASCs, ASC-A, Fibro, Fibro-A, iKC, and mature keratinocyte (mKC) derived from WT and $Asah1^{P361R/P361R}$ mice were quantified by FIA-ESI-MS/MS and LC-ESI-MS/MS. Statistically significant increases of total Cer were observed in iKC, mKC, ASC-A, and Fibro-A skin cells from $Asah1^{P361R/P361R}$ mice (Figure 6). These skin cell lines derived from $Asah1^{P361R/P361R}$ mice showed variable composition of accumulated Cer species differing in fatty acid chain length consistent with our observations of whole skin extracts. $Asah1^{P361R/P361R}$ ASC-A cells displayed statistically elevated C16:0, C18:0, C20:0, C22:0, C22:1, C24:0, C24:1, and C24:2 Cers (Figure 6B–L). $Asah1^{P361R/P361R}$ Fibro-A cells displayed statistically significant elevations C18:0, C20:0, C22:0, and C22:1 Cers (Figure 6B–L). $Asah1^{P361R/P361R}$ iKC cells displayed statistically significant elevations C14:0, C16:0, C24:0, C26:0, and C26:1 Cers (Figure 6B–L). $Asah1^{P361R/P361R}$ mKC cells displayed statistically elevated C14:0, C24:0, C26:0, and C26:1 Cers (Figure 6B–L). Although $Asah1^{P361R/P361R}$ ASCs and fibroblasts showed a slight increase in the Cer species we tracked, none were statistically significant (Figure 6B–L). Other lipids such as SM, MHC, DHC, Chol, and CholE were found to be similar to that observed in WT mice (Figure S4).

We also analyzed several hydroxyl-species of Cer in extracts from the same cells (Figure S5). Similar to whole skin extracts, the greatest increases were seen in C24:0-OH and C24:1-OH with the largest increases seen in fibroblasts and Fibro-A. Interestingly, although fibroblasts did not show statistically significant buildup of nonhydroxyl-Cer species, they accumulated considerable hydroxyl-Cer species with increased C22:0-OH, C26:0-OH, and C26:1-OH compared with controls (Figure S5).

4 | DISCUSSION

FD is a rare and multisystemic disorder caused by ACDase deficiency. FD patients display clinical variability with symptoms including painful deformed joints, subcutaneous nodules, hoarseness of voice, and progressive respiratory and neurologic involvement. Clinical reports have described abnormal skin development in FD patients including the appearance of skin nodules and lesions, as well as the formation of "Farber" and "Zebra" bodies under microscopic examination.[4,26] Stiff skin has been reported in at least one FD patient.[27] The condition started at birth with the patient displaying progressive joint contractures and thick indurated skin across the entire body resulting in limited joint mobility. That patient's neck was stiff, and a skin biopsy revealed accumulation of large foamy histiocytes within the fat lobules of the subcutaneous tissue. Although we did not observe skin lesions in our $Asah1^{P361R/P361R}$ FD mouse model, stiff neck skin and the accumulation of abnormal structures and histiocytes was prominent in these mice. Here, we performed a detailed histological and ultrastructural examination of the skin in $Asah1^{P361R/P361R}$ mice revealing foamy histiocytes and enlarged lysosomes mainly in the dermal reticular layer spreading to the connective tissue of the hypodermis in aging mice. By the age of 9 weeks a near complete loss of hypodermal AT was noted, a histological observation likely contributing to declining health.

The skin is rich in a broad range of bioactive lipids critical to the formation and maintenance of the epidermal barrier.[28–30] The composition of the stratum corneum, the uppermost thick layer, differs strongly from that of living cell membranes with ceramides (50%), cholesterol (25%), and free fatty acids (10%–15%) as the main lipid classes.[28] The role of Cer in stratum corneum is widely recognized and the lipid composition of diseased skin is often characterized by altered levels of Cer and the associated development of water barrier dysfunction in patients with atopic dermatitis, psoriasis, contact dermatitis, and some genetic disorders.[28–31] Moreover, epidermal 1-O-acylceramides (1-OACs) are upregulated during the establishment of the water permeability barrier in mice and must be tightly regulated as overexpression results in barrier dysfunction.[32] Teasing out 1-OAC molecular regulation and the effect of its modulation on skin barrier defects has proven challenging due to the numbers of enzymes involved, possibly redundant enzyme roles, and the contribution of other acyltransferases expressed in the epidermis.[32,33]

Our findings in whole skin extracts from $Asah1^{P361R/P361R}$ mice were dominated by the massive accumulation of

all studied Cer species (mainly C16:0) along with other neutral GSL that represent important products in the biosynthesis of more complex GSL from Cer. Individual skin cell lines from $Asah1^{P361R/P361R}$ mice showed variable composition of Cer species differing in fatty acid chain length. Increased Cer was most prominent in KC, although ASC-A and Fibro-A were also significantly altered. While fibroblasts did not accumulate nonhydroxy-Cer species, they did demonstrate significant hydroxyl-Cer buildup.

Fibroblasts along with ASC were the main cells affected by decreased proliferation over time in culture and they also displayed an increased inflammatory phenotype. Cer is widely recognized as an important secondary messenger in various stress responses and growth mechanisms.[34–36] Short-chain Cer alters cellular function in epidermal cells including KC and melanocytes.[36] Nonhydroxylated Cer species are important mediators of immune cell regulation.[36,37] Accumulated hydroxyl-Cer species in $Asah1^{P361R/P361R}$ mice could therefore be responsible for the altered proliferation of fibroblasts and ASC. The role of ACDase in cell proliferation has previously been described in MCF7 cells.[38] Treatment of MCF7 cells with Ceranib-2, a small molecule ACDase inhibitor, led to decreased viability in a dose-dependent and time-dependent manner attributed to the mitochondrial apoptosis pathway. Our findings support this as elevation of C16:0 Cer, also the main accumulated Cer species in FD, is known to induce apoptosis through the BAK and BAC proteins in the mitochondria-associated membrane.[39]

Interestingly, SPH was elevated in 9-week-old $Asah1^{P361R/P361R}$ mice. SPH, its derivatives, and their corresponding ceramides are natural antimicrobial agents.[40] They protect skin from bacterial colonization, and play an important role in antimicrobial defense, maintenance and integrity of lipid lamellae, and regulation of cell proliferation and differentiation. Interestingly, C18-SPH but not C18-dh-SPH is elevated in the stratum corneum of both an atopic dermatitis mouse model as well as from atopic dermatitis patient lesional skin.[40,41] SPH and dh-SPH play a structural role in stabilizing the skin barrier, and it is thought that their ratio must be closely maintained for normal stratum corneum formation.[41] The accumulation of SPH and resultant altered SPH/dh-SPH ratio could contribute to the increased thickness of the epidermal stratum corneum seen in our $Asah1^{P361R/P361R}$ mice.

The JAK/STAT3 signaling pathway is involved in various physiological processes, including immune function, cell growth, differentiation, and proliferation.[42,43] We previously showed increased phosphorylated STAT3 and NF-κB in liver lysates from $Asah1^{P361R/P361R}$ mice.[9] As both were found increased in skin lysates, we further investigated inflammatory signaling pathways in $Asah1^{P361R/P361R}$ mice and identified IL-6/JAK/STAT3 and alternative (noncanonical) NF-κB pathway

activation. A well-characterized function of the noncanonical NF-κB pathway is to mediate the development and architectural organization of primary and secondary lymphoid organs, including the spleen, lymph nodes, and thymus.[44,45] These organs have also been previously noted to display poor development in our $Asah1^{P361R/P361R}$ mice[6] suggesting an important role for the alternative (noncanonical) NF-κB pathway in normal lymphoid organ development. JAK/STAT3 is commonly activated during early immune responses.[43] We observed activation of JAK/STAT3 in FD-ASC but not in adipocytes or fibroblasts; thus activation of JAK/STAT3 signaling in FD-ASC may also play a role in their impaired differentiation into adipocytes. Although over 60 different cytokines and growth factors can activate the STAT signaling pathway, the IL-6 pathway is more clearly defined.[46] We identified increased IL-6 and MCP-1 release in media collected from isolated/cultured $Asah1^{P361R/P361R}$-AT cells that are composed not only of pre-adipocytes and adipocytes (partly) but by a large variety of immune cells including monocytes/macrophages. Because both cytokines were not increased in media collected from cultured ASC and fibroblasts alone, nor adipocytes differentiated from these cells in vitro, our results suggest that monocytes/ macrophages may be the main immune cells responsible for activation of IL-6/JAK/STAT3. This is also supported by the increased presence of monocyte/macrophages within isolated $Asah1^{P361R/P361R}$-AT measured by flow cytometry. As well, both IL-6 and MCP-1 are known to be released by macrophages.[47] Moreover, MCP-1 is a key chemokine regulating the migration and infiltration of monocyte/macrophages out of the bone marrow and into the circulation. The high expression of MCP-1 seen in these cells parallels that seen in the plasma of $Asah1^{P361R/P361R}$ mice and patients.[48]

In conclusion, this is the first in-depth analysis of the skin in an ACDase deficient animal model. We report that ACDase deficiency resulted in abnormal skin structure, owing to modified lipid composition and activation of the IL-6/JAK/STAT3 and (noncanonical) NF-κB pathways as well as ceramide pathway changes in these mice. Our findings follow up on previous case reports of FD patients with stiff skin syndrome and skin lesions. These data bring new insight to the molecular mechanisms behind the development of FD and may be of help in diagnosing and developing therapeutic approaches for the treatment of this disorder.

AUTHOR CONTRIBUTIONS

CONFLICT OF INTEREST
Jitka Rybova, Ladislav Kuchar, Jakub Sikora, William M. McKillop, and Jeffrey A. Medin declare no conflicts of interest pertaining to this study.

DATA AVAILABILITY STATEMENT
Data supporting the findings of this study are available from the corresponding author upon reasonable request.

INFORMED CONSENT
This article does not contain studies involving human subjects.

ANIMAL RIGHTS
Animal husbandry and usage was approved by the MCW Institutional Animal Care and Use Committee.

ORCID
Jitka Rybova https://orcid.org/0000-0002-4779-638X
Ladislav Kuchar https://orcid.org/0000-0003-0721-6624
Jakub Sikora https://orcid.org/0000-0003-4104-2023
William M. McKillop https://orcid.org/0000-0001-9683-7339
Jeffrey A. Medin https://orcid.org/0000-0001-8165-8995

REFERENCES
1. Yu FPS, Amintas S, Levade T, Medin JA. Acid ceramidase deficiency: Farber disease and SMA-PME. *Orphanet J Rare Dis.* 2018;13:121. doi:10.1186/s13023-018-0845-z
2. Moser HW, Linke T, Fensom AH, et al. Acid ceramidase deficiency: Farber lipogranulomatosis. In: Scriver CR, ed. *The metabolic and molecular bases of inherited disease.* 8th ed. McGraw-Hill; 2001:3573-3585.
3. Antonarakis SE, Valle D, Moser HW, Moser A, Qualman SJ, Zinkham WH. Phenotypic variability in siblings with Farber disease. *J Pediatr.* 1984;104:406-409. doi:10.1016/s0022-3476(84)81106-3
4. Schmoeckel C. Subtle clues to diagnosis of skin diseases by electron microscopy. "Farber bodies" in disseminated lipogranulomatosis (Farber's disease). *Am J Dermatopathol.* 1980;2:153-156. doi:10.1097/00000372-198000220-00011
5. Chedrawi AK, Al-Hassnan ZN, Al-Muhaizea M, et al. Novel V97G ASAH1 mutation found in Farber disease patients: Unique appearance of the disease with an intermediate

6. Alayoubi AM, Wang JC, Au BC, et al. Systemic ceramide accumulation leads to severe and varied pathological consequences. *EMBO Mol Med.* 2013;5:827-842. doi:10.1002/emmm.201202301
7. Sikora J, Dworski S, Jones EE, et al. Acid ceramidase deficiency in mice results in a broad range of central nervous system abnormalities. *Am J Pathol.* 2017;187:864-883. doi:10.1016/j.ajpath.2016.12.005
8. Yu FPS, Islam D, Sikora J, et al. Chronic lung injury and impaired pulmonary function in a mouse model of acid ceramidase deficiency. *Am J Physiol Lung Cell Mol Physiol.* 2018;314:L406-L420. doi:10.1152/ajplung.00223.2017
9. Yu FPS, Molino S, Sikora J, et al. Hepatic pathology and altered gene transcription in a murine model of acid ceramidase deficiency. *Lab Invest.* 2019;99:1572-1592. doi:10.1038/s41374-019-0271-4
10. Yu FPS, Sajdak BS, Sikora J, et al. Acid ceramidase deficiency in mice leads to severe ocular pathology and visual impairment. *Am J Pathol.* 2019;189:320-338. doi:10.1016/j.ajpath.2018.10.018
11. Hartree EF. Determination of protein: A modification of the Lowry method that gives a linear photometric response. *Anal Biochem.* 1972;48:422-427. doi:10.1016/0003-2697(72)90094-2
12. Natomi H, Sugano K, Iwamori M, Takaku F, Nagai Y. Region-specific distribution of glycosphingolipids in the rabbit gastrointestinal tract: Preferential enrichment of sulfoglycolipids in the mucosal regions exposed to acid. *Biochim Biophys Acta.* 1988;961:213-222.
13. Musalkova D, Majer F, Kuchar L, et al. Transcript, protein, metabolite and cellular studies in skin fibroblasts demonstrate variable pathogenic impacts of NPC1 mutations. *Orphanet J Rare Dis.* 2020;15:85. doi:10.1186/s13023-020-01360-5
14. Liebisch G, Binder M, Schifferer R, Langmann T, Schulz B, Schmitz G. High throughput quantification of cholesterol and cholesteryl ester by electrospray ionization tandem mass spectrometry (ESI-MS/MS). *Biochim Biophys Acta.* 2006;1761:121-128. doi:10.1016/j.bbalip.2005.12.007
15. Kuchar L, Ledvinova J, Hrebicek M, et al. Prosaposin deficiency and saposin B deficiency (activator-deficient metachromatic leukodystrophy): Report on two patients detected by analysis of urinary sphingolipids and carrying novel PSAP gene mutations. *Am J med Genet A.* 2009;149A:613-621. doi:10.1002/ajmg.a.32712
16. Kuchar L, Sikora J, Gulinello ME, et al. Quantitation of plasmatic lysosphingomyelin and lysosphingomyelin-509 for differential screening of Niemann-Pick A/B and C diseases. *Anal Biochem.* 2017;525:73-77. doi:10.1016/j.ab.2017.02.019
17. Zhang Y, Tong D, Mishra A, et al. Isolation and patch-clamp of primary adipocytes. *Methods Mol Biol.* 2017;1566:145-150. doi:10.1007/978-1-4939-6820-6_14
18. Aune UL, Ruiz L, Kajimura S. Isolation and differentiation of stromal vascular cells to beige/brite cells. *J Vis Exp.* 2013. doi:10.3791/50191
19. Zhang LJ. Isolation, culture, and characterization of primary mouse epidermal keratinocytes. *Methods Mol Biol.* 2019;1940:205-215. doi:10.1007/978-1-4939-9086-3_15

20. Asfaw B, Schindler D, Ledvinova J, et al. Degradation of blood group a glycolipid A-6-2 by normal and mutant human skin fibroblasts. *J Lipid Res.* 1998;39:1768-1780.

21. Rybova J, Ledvinova J, Sikora J, et al. Neural cells generated from human induced pluripotent stem cells as a model of CNS involvement in mucopolysaccharidosis type II. *J Inherit Metab Dis.* 2018;41:221-229. doi:10.1007/s10545-017-0108-5

22. Maru GB, Gandhi K, Ramchandani A, et al. The role of inflammation in skin cancer. *Adv Exp med Biol.* 2014;816:437-469. doi:10.1007/978-3-0348-0837-8_17

23. Dondelinger Y, Jouan-Lanhouet S, Divert T, et al. NF-kappaB-independent role of IKKalpha/IKKbeta in preventing RIPK1 kinase-dependent apoptotic and Necroptotic cell death during TNF signaling. *Mol Cell.* 2015;60:63-76. doi:10.1016/j.molcel.2015.07.032

24. Bista P, Zeng W, Ryan S, Bailly V, Browning JL, Lukashev ME. TRAF3 controls activation of the canonical and alternative NFkappaB by the lymphotoxin beta receptor. *J Biol Chem.* 2010;285:12971-12978. doi:10.1074/jbc.M109.076091

25. McLafferty E, Hendry C, Alistair F. The integumentary system: Anatomy, physiology and function of skin. *Nurs Stand.* 2012; 27:35-42. doi:10.7748/ns2012.10.27.7.35.c9358

26. Bao XH, Tian JM, Ji TY, Chang XZ. A case report of childhood Farber's disease and literature review. *Zhonghua Er Ke Za Zhi.* 2017;55:54-58. doi:10.3760/cma.j.issn.0578-1310.2017.01.011

27. El-Kamah GY, El-darouti MA, Kotoury AIS, Mostafa MI. Farber disease overlapping with stiff skin syndrome: Expanding thr spectrum. *Egypt J Med Hum Genet.* 2009;10:97-104.

28. Kendall AC, Kiezel-Tsugunova M, Brownbridge LC, Harwood JL, Nicolaou A. Lipid functions in skin: Differential effects of n-3 polyunsaturated fatty acids on cutaneous ceramides, in a human skin organ culture model. *Biochim Biophys Acta Biomembr.* 2017;1859:1679-1689. doi:10.1016/j.bbamem.2017.03.016

29. Kendall AC, Pilkington SM, Massey KA, Sassano G, Rhodes LE, Nicolaou A. Distribution of bioactive lipid mediators in human skin. *J Invest Dermatol.* 2015;135:1510-1520. doi:10.1038/jid.2015.41

30. Sjovall P, Skedung L, Gregoire S, et al. Imaging the distribution of skin lipids and topically applied compounds in human skin using mass spectrometry. *Sci Rep.* 2018;8:16683. doi:10.1038/s41598-018-34286-x

31. Choi MJ, Maibach HI. Role of ceramides in barrier function of healthy and diseased skin. *Am J Clin Dermatol.* 2005;6:215-223. doi:10.2165/00128071-200506040-00002

32. Rabionet M, Bernard P, Pichery M, et al. Epidermal 1-O-acylceramides appear with the establishment of the water permeability barrier in mice and are produced by maturing keratinocytes. *Lipids.* 2022;57:183-195. doi:10.1002/lipd.12342

33. Bayerle A, Marsching C, Rabionet M, et al. Endogenous levels of 1-O-acylceramides increase upon acidic ceramidase deficiency and decrease due to loss of Dgat1 in a tissue-dependent manner. *Biochim Biophys Acta Mol Cell Biol Lipids.* 2020;1865: 158741. doi:10.1016/j.bbalip.2020.158741

34. Hannun YA, Obeid LM. The ceramide-centric universe of lipid-mediated cell regulation: Stress encounters of the lipid kind. *J Biol Chem.* 2002;277:25847-25850. doi:10.1074/jbc.R200008200

35. Masukawa Y, Narita H, Shimizu E, et sal. Characterization of overall ceramide species in human stratum corneum. *J Lipid Res.* 2008;49:1466-1476. doi:10.1194/jlr.M800014-JLR200

36. Uchida Y. Ceramide signaling in mammalian epidermis. *Biochim Biophys Acta.* 2014;1841:453-462. doi:10.1016/j.bbalip.2013.09.003

37. Chalfant CE, Spiegel S. Sphingosine 1-phosphate and ceramide 1-phosphate: Expanding roles in cell signaling. *J Cell Sci.* 2005; 118:4605-4612. doi:10.1242/jcs.02637

38. Vejselova D, Kutlu HM, Kus G. Examining impacts of ceranib-2 on the proliferation, morphology and ultrastructure of human breast cancer cells. *Cytotechnology.* 2016;68:2721-2728. doi:10.1007/s10616-016-9997-7

39. Grosch S, Schiffmann S, Geisslinger G. Chain length-specific properties of ceramides. *Prog Lipid Res.* 2012;51:50-62. doi:10.1016/j.plipres.2011.11.001

40. Loiseau N, Obata Y, Moradian S, et al. Altered sphingoid base profiles predict compromised membrane structure and permeability in atopic dermatitis. *J Dermatol Sci.* 2013;72:296-303. doi:10.1016/j.jdermsci.2013.08.003

41. Toncic RJ, Jakasa I, Hadzavdic SL, et al. Altered levels of sphingosine, Sphinganine and their ceramides in atopic dermatitis are related to skin barrier function, disease severity and local cytokine milieu. *Int J Mol Sci.* 2020;21(6):1958. doi:10.3390/ijms21061958

42. Niwa Y, Kanda H, Shikauchi Y, et al. Methylation silencing of SOCS-3 promotes cell growth and migration by enhancing JAK/STAT and FAK signalings in human hepatocellular carcinoma. *Oncogene.* 2005;24:6406-6417. doi:10.1038/sj.onc.1208788

43. Johnson DE, O'Keefe RA, Grandis JR. Targeting the IL-6/JAK/-STAT3 signalling axis in cancer. *Nat Rev Clin Oncol.* 2018;15: 234-248. doi:10.1038/nrclinonc.2018.8

44. Weih F, Caamano J. Regulation of secondary lymphoid organ development by the nuclear factor-kappaB signal transduction pathway. *Immunol Rev.* 2003;195:91-105. doi:10.1034/j.1600-065x.2003.00064.x

45. Sun SC. The noncanonical NF-kappaB pathway. *Immunol Rev.* 2012;246:125-140. doi:10.1111/j.1600-065X.2011.01088.x

46. Schwartz DM, Bonelli M, Gadina M, O'Shea JJ. Type I/II cytokines, JAKs, and new strategies for treating autoimmune diseases. *Nat Rev Rheumatol.* 2016;12:25-36. doi:10.1038/nrrheum.2015.167

47. Appari M, Channon KM, McNeill E. Metabolic regulation of adipose tissue macrophage function in obesity and diabetes. *Antioxid Redox Signal.* 2018;29:297-312. doi:10.1089/ars.2017.7060

48. Dworski S, Lu P, Khan A, et al. Acid ceramidase deficiency is characterized by a unique plasma cytokine and ceramide profile that is altered by therapy. *Biochim Biophys Acta Mol Basis Dis.* 2017;1863:386-394. doi:10.1016/j.bbadis.2016.11.031

SUPPORTING INFORMATION

Additional supporting information can be found online in the Supporting Information section at the end of this article.